To what extent have laterites contributed to the geochemical, surface reflectance and magnetic properties of adjacent tropical soils? Evidence from Niger and Burkina Faso.

Hunt, A.[1], Oldfield, F.[2], Bloemendal, J.[2], Boyle, J.F.[2], Chiverrell, R.C.[2], Lyons R.[3], Shen, Z.[4], Williams, E.R..[5] Balsam, W.[6]

[1] Department of Earth and Environmental Sciences, University of Texas at Arlington, Arlington, Texas USA

[2] School of Environmental Sciences, University of Liverpool, Liverpool, UK.

[3] 130 Holm Lane, Prenton, Wirral, Merseyside, CH43 2HT, UK

[4]Department of Marine Science, Coastal Carolina University, PO Box 261954 Conway, SC 29528, USA.

[5] Parsons Laboratory, Massachusetts Institute of Technology, Cambridge, MA 02139-4307, USA.

[6] Department of Earth Science, Dartmouth College, Hanover, NH 03755, USA

Corresponding author: F. Oldfield, oldfield.f@gmail.com Tel: 44(0) 151 632 6154

Abstract

The present study is based on a suite of surface samples from exposures of eroded laterite, considered to be Tertiary in age, and nearby soils in the Sahelian region of SW Niger and Burkina Faso. X-Ray Fluorescence (XRF), X-Ray Diffraction (XRD), Computer Controlled Scanning Electron Microscopy (CCSEM), Energy Dispersive X-ray Spectroscopy (EDS), Diffuse UV/Visual Reflectance Spectroscopy (DRS) and a suite of magnetic measurements have been used to shed light on the origin of the soils and their possible derivation from the adjacent, eroded laterite outcrops. On the basis of the wide range of data obtained, we conclude that the mineralogy and magnetic properties of the soils precludes direct derivation from the laterites without further weathering and modification. Nor does the evidence support the view that the soils have evolved entirely independently, uninfluenced by input from the laterites.

The only conclusion that is consistent with all the lines of evidence is that the erosion of the laterites provided at least a significant part of the material upon which soil formation took place. This must have occurred at a time early enough to permit a long period of subsequent soil development during which the iron oxides, specifically haematite and ferrimagnetic minerals, were significantly modified. From this, we infer that eroded material from discontinuous laterite exposures has contributed significantly to the remotely sensed, distinctive reflectance characteristics of the Sahel surfaces. The magnetic properties of the soils provide evidence for the *in situ* neo-formation of fine, secondary, pedogenic magnetite/maghemite grains typical of those found in many soils across the Sahel region and elsewhere in both temperate and tropical environments.

Key words: laterites, Sahel, reflectance, magnetic properties, soil formation.

Introduction

The geochemistry, reflectance characteristics (albedo) and magnetic properties (Lyons et al. 2010; 2012, Grey et al. 2005; Williams et al. 2009) of the Sahel region raise several related questions regarding the relationship between the widespread occurrence of laterites and the dominantly red-coloured soils of the Sahel. In order to explore these further, comparisons have been made between laterite and adjacent soil samples (Fig. 1) along a transect from Niamey in Niger to Ouagadougou in Burkina Faso (Fig. 2). Whether classified as soils or metasomatic rocks (Aleva 1994), laterites are the product of intensive and long lasting tropical weathering. The time frame inferred for laterite formation is not well constrained and varies from 150Ma (Tardy et al. 1991) to 24-25 Ma (Gunnell 2003), the latter estimate based on radiometric evidence. The deep red-brown laterites in the region sampled are typically enriched in Fe oxides and fall within the type classified as ferricretes by Tardy et al. (1995), though their autochthonous origin through *in-situ* weathering of the igneous bedrock would lead Widdowson (2007) to preclude this assignation on the basis of his genetic classification. Such laterites are greatly enriched in haematite as a result of the leaching processes that they have experienced over millions of years. Haematite is one of the least soluble minerals found in the regolith anywhere in the world. The discontinuous outcrops with their eroded edges suggest that the

present exposures of laterite are residual from previously much more extensive and continuous cover. The soil samples analyzed all come from within 10 to 30 m of the edge of the adjacent, sampled laterite outcrops and share the deep red-brown colouration of much of the surface material across the Sahel (Fig. 1). The questions posed at the outset are threefold:

(i) To what extent have the geochemical properties of the soils been derived from the nearby laterite exposures and, if so, on what kind of timescale? Since both the laterites and soils must have been formed from the underlying acid igneous rocks one possibility is that they have developed quite independently on different timescales, each under a different range of climatic conditions. If, on the other hand, the soils have developed in part or whole on eroded material derived from laterite outcrops, the question becomes partly one of timing. Does the evidence point to recent erosion from the existing exposures with no significant chemical transformation, or to the effects of long-term denudation processes in which the products of laterite erosion have contributed significantly to the substrate upon which the present-day soils have evolved in response to the then prevailing and subsequent climatic conditions?

(ii) In this regard, particular attention is paid to evidence for the origin of the haematite component in the soils, in light of the importance of haematite in controlling the red colour, hence the reflectance qualities of the surface soils. Remote sensing using MODIS and AATSR (Grey et al. 2005; Schaaf, personal communication, 2009; Williams et al. 2009.) confirms a strong contrast in reflectance between Sahel and Sahara surfaces. Formenti et al. (2014a) also demonstrate the distinctive reflectance characteristics resulting from the high haematite+ goethite concentrations in the local Sahel dusts. Here we explore the extent to which the soil haematite, largely responsible for the distinctive surface reflectance, is a consequence of the erosion of laterite outcrops, or of independent pedogenesis.

(iii) Thirdly, even if soils may have been derived from the nearby laterites, to what extent are the magnetic properties themselves inherited from the laterites, rather than generated through pedogenesis? Since Zhou et al. (1990) demonstrated that the sequence of alternating magnetic susceptibility values in Quaternary sections from the Chinese Loess Plateau reflected predominantly the pedogenic

97 enhancement of susceptibility in palaeosols, there has been considerable interest in
98 the link between soil magnetic susceptibility and rainfall. Many studies have been
99 published in the wake of Maher and Thompson's (1992) pioneering analysis
100 confirming the positive relationship between those two quantities and hence the
101 potential for using susceptibility records as proxies for past variations in precipitation.
102 Recently, broadly based summaries by Balsam et al. (2011) and Maher and Possolo
103 (2013) have served to confirm the validity of the link. Balsam et al. (2011) present
104 robust statistical evidence for the strength of the relationship ($r^2 = 0.611$) across
105 strong rainfall gradients in tropical Africa in the form of a suite of samples from Mali,
106 where Lyons et al. (2010; 2012) had previously pointed to soil susceptibility
107 variations reflecting the rainfall gradient across the Sahel-Sahara Transition.
108 Subsequent analysis of a larger data set, less strongly dominated by samples from
109 transects spanning the clear north-south rainfall gradients, failed to demonstrate the
110 same strong link between rainfall and susceptibility (Oldfield et al. 2014). One
111 possible factor contributing to the weaker relationship is the role that eroded laterite
112 may have played in controlling the magnetic properties of adjacent soils. Should this
113 turn out to be the case, it would cast doubt on the inferred pedogenic origin of the
114 apparent susceptibility:rainfall link across the Sahel-Sahara transition and on the
115 inferences based on this putative link (Lyons et al. 2010, 2012; Balsam et al. 2011).
116 The Sahel region is unique in Africa with respect to the high prevalence of laterite
117 surfaces (Gunnel 2003; Burke and Gunnell 2008) and the strong occurrence of iron
118 oxides (Formenti et al. 2014 a, b).

119 Six lines of evidence have been used to shed light on these questions – (i) element
120 concentrations determined by X-Ray Fluorescence (XRF) in order to assess the
121 degree of similarity or otherwise in the presence and concentrations of chemically
122 relatively stable elements; (ii) mineralogy determined by X-Ray Diffraction (XRD)
123 with a view to exploring possible differences between the laterites and soils,
124 especially with regard to the iron oxides recorded; (iii) haematite and goethite signals
125 and ratios derived from Diffuse Reflectance Spectroscopy (DRS) with special
126 emphasis on the quantitative and qualitative information derived from the spectra for
127 haematite in adjacent laterite and soil samples; (iv) sample imaging and particle
128 characterization using Computer-Controlled Scanning Electron Microscopy
129 (CCSEM); (v) linked to the latter, Energy Dispersive X-ray Spectroscopy (EDS) in

order to allow both geochemical and visual comparisons on the basis of individual particles and particle classes; and (vi) magnetic measurements with a view to addressing the third question posed above.

Environmental setting and sampling

The samples from the transect (Fig. 2) come from an area with a gradient in mean annual rainfall from 500 mm in the northern part of the Transect, to 750 mm in the south. The rainy season is between June and September but subject to extreme inter-annual and inter-decadal variability. Most of the soils and laterites are underlain by acid, igneous basement rocks, mainly granites and migmatites. The soils over the transect are mainly classified as lixisols (Deckers et al. 1998; FAO, 2006), which are typically developed on old landscapes with a tropical climate experiencing a pronounced dry season. They are strongly weathered soils in which clay has been eluviated from the surface to form a kaolinitic subsurface horizon (FAO, 2006). Haematite enrichment (rubefaction) through dehydration of iron compounds during the dry season is typical and enrichment by aeolian deposition has been inferred for some lixisols (World Soil Information, undated). Samples all came from the top ~5cm of the exposures. In the case of the soils, this meant that in most cases, the sand-rich eluvial horizon alone was sampled, except where deflation had removed surface material (site 4a). Samples were stored in Ziploc plastic bags.

Methods of Sample Analysis

Element analysis by X-Ray Fluorescence

XRF analyses were undertaken on finely ground samples with a Bruker S2 Ranger energy dispersive x-ray fluorescence analyser, using a Pd X-ray tube and Peltier-cooled silicon drift detector. The instrument was run under three different measurement conditions (20, 40 and 50 keV tube excitement) on loose powder (1 to 3 g) under helium. Powder cups were prepared with spectroscopic grade 6 µm polypropylene film (Chemplex Cat. No. 425). Calibration used a set of up to 18 certified reference materials. Mass attenuation correction used theoretical alphas, with organic matter concentrations estimated by loss-on-ignition.

Computer-Controlled Scanning Electron Microscopy (CCSEM +EDS)

The microscopic constituents of laterite and soil samples were characterized at the individual particle (IP) level using a combination of scanning electron microscopy (SEM) and energy dispersive X-ray spectroscopy (EDS). Finely divided material from each sample was prepared for CCSEM analysis in the following way: (i) A subsample of material (<0.5 mg) was placed in a 100 mL test tube containing 75 mL of MiliQ water to which a small amount (<0.5 ml) of surfactant (polysorbate 20) was added; this was then ultrasonically agitated for 5 minutes. (ii) A series of aliquots of increasing volume (from 0.1-0.5 mL) of the soil in water suspension were filtered from a chimney reservoir containing MiliQ water, onto a 25 mm diameter 0.4 µm pore size polycarbonate membrane filter. (iii) Several filters were prepared so a desirable filter loading could be selected. A filter loading with a separation between particles of at least one particle diameter was considered suitable; however, a filter with a lighter loading was preferred. (iii) Each filter was attached to an SEM mount with an intervening layer of adhesive carbon paint before it was submitted for final review and CCSEM analysis.

An FEI/Aspex Personal Scanning Electron Microscope (PSEM) was used to perform Computer-Controlled Scanning Electron Microscopy (CCSEM). Backscattered electron (BE) collection was used for particle imaging. Variations in BE yield correlate with particle average atomic number, thus permitting particle selection based on composition (Goldstein et al. 2003). Particle element composition was determined by EDS using an OmegaMax™ silicon drift detector with an ultra-thin window, permitting the detection of light elements such as carbon, and oxygen. The PSEM was operated in variable pressure mode, which obviated the need to apply a conducting coat. CCSEM collected data under computer control and allowed the collection of statistically significant data sets in a time efficient manner. To facilitate this, sub-samples of particles from the study locations were vacuum-filtered onto separate 25 mm diameter, 0.4 µm polycarbonate filters. Operating under computer-controlled IP analysis of the material on a filter proceeded sequentially in a particle detect mode and then in particle measurement mode. A BE image threshold was initially set so that the particles were isolated from the carbon filter by greater BE yield. In the detect phase, the primary electron beam stepped over a field of view in

the SEM until a particle was registered (BE yield above the set threshold) and at this point the measurement process started. During the particle measurement phase the size, shape and element composition of a particle were determined as the primary electron beam rastered over the particle. After the measurement phase, the system returned to particle detect mode until another particle was detected. The standard operating conditions for the analyses were: an accelerating voltage of 25 keV, a beam current of approximately 1.0 nA, and a working distance of approximately 16 mm. While the X-ray spectrum for each particle was stored, data for a specified element list were captured for each particle. A “crustal” element list of Na, Mg, Al, Si, P, S, Cl, K, Ca, Ti, Mn, and Fe was used in the vector file in this study.

To interpret the CCSEM data, groups of “like” particles, based on element composition, were identified in the CCSEM data from the analysis of one of the soil samples as a training set. This focused on identifying homogenous groups of particle types using a supervised divisive hierarchical cluster analysis. The cluster analysis reached a stopping point where further division of a group was not necessary, or when a new group would consist of less than 1% of the total number of particles in the data set. Based on the composition of the particles in each group, a set of rules was defined to classify particles belonging to that group. The applied rules allowed for a “tight” classification of the particles. For example, for a single element particle (e.g., Si) the rule requirement was that the relative X-ray percentage for silicon had to be >98%. In the case of two or more elements the rule definition was that the sum of the relative X-ray percentage for all elements in the rule had to be >98% and each individual element had to be >3%. The only exception was for the presence or absence of Ti and Mn. These classes of rules were ordered in a linear fashion to allow classification attribution of CCSEM data from samples in this study. Here a 58-class scheme was formulated and ordered into a linear sorting scheme. Included at the end of the scheme was an extra class (Class 100: ‘other’), to which particles were assigned that were not captured by any of the preceding classes. Class 100 contained no rules for the assignment of particles to it, serving only to record the numbers of particles unassigned to any of the 58 classes. CCSEM data from the analysis of a new particle sample was sifted through the scheme and a particle was assigned to a class if its composition matched the rules defining the class.

X-Ray Diffraction (XRD)

Sample mineralogy was determined on finely ground samples by X-ray diffraction (XRD). The XRD patterns from samples 1, 1A, 3, 3A, 8A, 9, 9A, 11, 11A and 12A were collected with a Bruker D8 Advanced high resolution powder diffractometer with a Bragg-Brentano geometry and monochromatic Cu-Ka radiation. This employed a copper tube operating at 40 kV and 40 mA, fixed slit optics with incident beam divergence = 1°, receiving slit = 0.15 and NaI detector with pulse discrimination. In collecting data, the 2θ step size was 0.02°; the counting time per step was 2s; and the 2θ range = 2-90. For samples 4, 4A, 5, 5A, 6, 6A, 7, 7A, 8, 10 and 10A, X-ray diffraction was performed on a Shimadzu XRD-7000 X-ray diffractometer with a Cu X-ray tube. Sample mounts were scanned from 2-80^0 2θ at a scan speed of 2^0 2θ per minute. The system operated at 40 kV with a tube current of 30 mA in a continuous scan mode. The incident beam divergence was 1°, the scattering slit was 1°, and the receiving slit was 0.3 mm; the scintillation detector was a NaI single crystal activated with a small quantity of Tl.

Diffuse Reflectance Spectroscopy (DRS)

To estimate the relative concentrations of haematite and goethite in the samples we used established diffuse reflectance UV-VIS spectroscopy (DRS) methods (Deaton and Balsam 1991; Torrent and Barron, 2002; Torrent et al., 2007). Paired soil and laterite samples were dried, powdered (<10 μm) and pressed into pellets using a 15 tonne hydraulic press, before collection of the DRS spectra. The DRS spectra were recorded from 190 to 1100 nm in 0.5-nm steps at a scan rate of 30 nm min^{-1}, using a Thermo Evolution 300 UV-Vis Spectrophotometer equipped with a Praying Mantis Diffuse Reflectance Accessory (Thermo Scientific) that uses all-aluminium coated optics rather than traditional integrating spheres, thus allowing an extended optical range. The Praying Mantis allows a diffuse reflectance measurement on samples as small as 3 mm in diameter and 1 mm thickness. The spectrophotometer uses a Xenon flash light source and has a stated accuracy of +/-0.3nm over the recorded data range.

256 The First Derivative (D 1) of each spectrum was determined directly using the
257 method established by Deaton and Balsam (1991) and further evaluated in Balsam
258 et al. (2014). In determining the Second Derivative (D 2) (Scheinost et al. 1998;
259 Torrent et al. 2007), the spectrum of reflectance (R) was transformed using the
260 Kubelka-Munk (K-M) remission function [$F(R) = (1-R)^2/2R$)]. D 1 uses the peak
261 height of the spectrum close to 580nm as the basis for calculation (Fig. 9), and D 2
262 uses the amplitude of the difference in values between peak and trough (Fig. 10).
263 Balsam et al. (2014) show that in the case of haematite, D 1 is the more sensitive of
264 the two in light matrices.

265 The reliability of the analyses provided by the system was assessed by analysing a
266 training set of 25 soils ($r^2 = 0.88$) from the Mediterranean region with haematite and
267 goethite concentrations determined by XRD (Torrent and Barron, 2002). In the
268 present case, however, the inferred concentrations of iron oxides in many of the
269 samples greatly exceed those used in the calibration.

270 **Magnetic Measurements**

271 All samples were packed into 10ml plastic sample holders, immobilised using clean
272 cling film and subjected to a standard range of magnetic measurements comprising
273 low field susceptibility at both low (0.47 kHz; χ_{LF}) and high (4.7 kHz; χ_{HF})
274 frequencies, leading to the calculation of the frequency-dependent susceptibility as
275 the difference between the two, expressed here as a mass specific value (χ_{FD}) or as
276 a percentage of χ_{LF} (χ_{FD}%). Subsequently, the following laboratory remanence
277 measurements were carried out: Anhysteretic Remanent Magnetisation (ARM),
278 expressed as susceptibility of ARM (χ_{ARM}) 'Saturation' (1T) Isothermal Remanent
279 Magnetisation (SIRM) followed by DC reverse field demagnetisation in fields of -20
280 mT, -40 mT, -100 mT and -300 mT. These measurements also yielded the 'S' values
281 as shown in Figure 11. This sequence of measurements and calculations has
282 generally provided a good basis for the initial magnetic characterization and
283 discrimination of sample sets, whether of sediments (Oldfield, 2012), soils (Hao et
284 al., 2008) or dusts (Lyons et al., 2012). Details of instrumentation, methods and
285 measurements are given in Lyons et al. (2010) and their interpretation is considered
286 in more detail in Walden et al. (1999) and Maher (2011). In addition, six samples
287 were used for additional measurements. Stepwise IRM acquisition using 31 fields

between 15mT and 1T and subsequent model-based deconvolution (Heslop et al. 2002) were used to provide more detailed information on the remanence carriers present (Oldfield et al. 2014). The results are summarised in Table 5 and Figure 12.

Results

X-Ray Fluorescence (XRF)

XRF element concentrations were used to test whether the soil composition is consistent with partial derivation from the adjacent eroding laterite outcrops. In addition to total Fe, which includes both chemically resistant and soluble forms, we examined only elements that are generally resistant to chemical weathering and regarded as immobile in soil (Ti, Nb, Zr, Cr). Further, to avoid dilution signals, such as lowered element concentrations due to dilution by quartz (which may be selectively concentrated during soil forming processes, or by the loss of fines in the surface soils through wind erosion, or eluviation), we generated proportion diagrams for 20 of the samples, including all those from sites where paired soil and laterite samples were taken (Figure 3). These are analogous to triangular diagrams but have the vertical (trace element) axis exaggerated in scale to such an extent that the sides of the triangle show no perceptible narrowing.

The sample scatter shows almost complete separation of the soil and laterite samples, but with distributions that do not preclude a continuity of composition. Indeed, although scattered, the compositional variation of all samples (both soil and laterite) can be seen as differing mixtures of identical end members, one enriched in Si and Zr (which dominates the soil samples), and the other enriched in Nb, Ti and Cr (which dominates the laterites). Thus, from the XRF data, the soils appear to be compositionally consistent with their derivation from the same substrate as the laterites. Nor do these data alone preclude at least partial derivation of the soils from the nearby laterite outcrops.

Computer-Controlled Scanning Electron Microscopy (CCSEM)

Here we examine CCSEM-acquired data from the analysis of nine laterite and seven soil samples. There were three paired soil and laterite samples (Sites 5, 7 and 10 in Figure 2). Data at the individual particle level were obtained on between 2,061 and

7,586 particles per sample. The CCSEM data were sorted through the 58-class scheme and the results are set out in Tables 1 and 2. Many classes in the scheme were populated by less than 1% of the total number of particles analyzed in the sample. For the sake of brevity, we have reported only on the class assignments where ≥ 1% of the total number of particles were reported in a class. Out of the 58 classes this amounted to 20 classes populated by the soil particles and 15 populated by the laterite particles. The classes contained only inclusionary criteria (rules) defined by combinations of the pre-defined elements in a vector file. The most basic classes consisted of one element. For example the Si-only class had a rule for a particle composition of only Si (quartz). As the classification scheme employed a linear sort for class allocation, the compositionally more complex classes were positioned lower in the scheme order with Class 100 (other) accounting for particle types not captured in any of the 58 classes.

The soil and laterite samples yielded markedly different CCSEM classification results (Tables 1 and 2). For example, the diversity of particles types was much smaller in the laterites compared to the soils (occupying 13 vs. 18 classes). More tellingly, only two classes recorded particles from every one of the seven laterite samples examined (30 and 37), while four classes (1, 8, 30 and 37) recorded particles from every one of the seven soil samples examined. At the class level, most of the laterite particles (52-91% (average 74%) in the nine samples) occupied class 30 (Al-Si-Fe composition), and, fewer laterite particles (2 -15% from three samples (average 8%)) were recorded in class 8 (Al-Si). In contrast, soil particles from all samples were also assigned to classes 8 and 30, but there were substantially fewer soil (than laterite) particles in class 30 (44-58% (average 50%)), while a greater number of soil (than laterite) particles were recorded in class 8 (6-26% (average 12%)). Also, while soil particles populated classes 36 (Na-Al-Si-K), 47 (Mg-Al-Si-K-Fe), and 52 (Na-Al-Si-K-Fe), either none or a non-significant number of laterite particles was recorded in these classes. Examples of soil particles with these compositions plus an example of a soil particle with an Al-Si composition (class 8) are set out in Figure 4. Iron is highly abundant in the soils and the laterites, although less abundant as Fe-only particles (as oxides, etc.). CCSEM shows that such particles were present as irregular fragments in both soils and laterites (e.g., Fig. 5c), and rarely was any crystal habit observed. Some exceptions are documented in Figure 5. Goethite after

pyrite was observed in one of the soils (Fig. 5a), and botryoidal haematite was observed in a laterite (fig. 5d). In addition, micrometre-sized stellate crystals composed of Fe were observed in the soil (Fig. 5b).

On an individual particle basis, while there was a marked difference in the number of soil particles compared to laterite particles assigned to class 30 (Al-Si-Fe), there were also differences in the relative proportions of the elements that constitute these particles. Consistently, there was a greater proportion of Fe in the laterite particles than in the soil particles assigned to class 30. This was most obvious when class 30 element concentrations (for Al, Si, and Fe) were extracted from the laterite and soil CCSEM data sets, and graphed on ternary plots. The clearest examples of these differences were provided by the class 30 data for soil 6 (Fig. 6a) and laterite 0 (Fig. 6b). While there are some high Fe concentration particles in class 30 for soil sample 6A, the trend is towards a cluster of high Si and Al and low Fe particles. In contrast, the majority of class 30 particles identified in laterite sample 0A had high Fe and low Al and Si concentrations. It is perhaps worth noting that the abundance of class 8 (Al and Si) particles in the laterites is less than in the soils and precipitation of Fe, because it is enriched in the laterites, may lead to a higher Fe content in the Al-Si-Fe laterite particles. The element concentration differences between soil and laterite class 30 particles were underscored by morphological differences revealed by a visual examination in the SEM. Examples of Al-Si-Fe particles from soil sample 10A are presented in Figure 7 (a-d). These particles with lower Fe content are sub-angular to rounded in shape, and the BE contrast of the surfaces are consistently uneven with brighter areas exhibiting higher Fe levels. In contrast, the high Fe content examples of Al-Si-Fe particles from laterite sample 10A (Figure 8a-d) display an angular form, and generally have an unvarying BE contrast.

X-Ray diffraction (XRD)

Samples were provided for XRD analysis in the hope that this technique would help to establish the mineralogical basis for any differences between the laterite and soil samples. Table 3 summarizes the XRD data from 10 laterite and 11 soil samples. The data for samples 1 (1A), 3 (3A), 4 (4A), 5, 5A), 6, (6A), 7 (7A), 8 (8A), 9 (9A),10 (10A) and 11 (11A) are from adjacent laterites and (soils).

Comparison of spectra with reference samples using RockJock (Eberl, 2003) unambiguously identifies the quartz in all samples, and kaolinite (ordered rather than disordered) in all samples except for a single soil (Site 1). A reflection at 33.2°2θ (CuKα) cannot be attributed to either quartz or kaolinite, but is expected to be shown by both haematite (its largest expected reflection) and goethite (its third largest expected reflection). All other expected haematite and goethite reflections coincide with others from the more abundant quartz and kaolinite. The only possibility for independent verification of either haematite or goethite by XRD lies with reflections at 14.5 and 53.3° (goethite) and 54.4° (haematite), though all of these are partially compromised by reflections from kaolinite and quartz. These reflections correlate significantly with each other and with the 33.2° reflection (but not with reflections of quartz or kaolinite), suggesting that they are indeed reflections of haematite and/or goethite and that the occurrences of the two minerals are correlated. However, it must also be recognised that both minerals show a degree of variability, and the possibility cannot be ruled out that the 53.3° has been influenced by haematite alone and thus may not indicate the presence of goethite. The reflection at 14.5° unambiguously identifies goethite, but it is weak and thus poorly constrains its abundance.

In addition to quartz, kaolinite, and haematite/goethite, small reflections at 8.8° 2θ in three laterite and two soil samples (similar magnitude in both types of material) reveal erratic occurrences of a 10Å sheet silicate. Mica cannot be firmly ruled out, but there is no sign of the many large reflections commonly seen for biotite or muscovite, so illite is more likely.

All reflections present on the spectra are thus attributable to quartz, kaolinite, haematite/goethite and “illite”. Other minerals, if present, must make up less than about 1 weight percent of the material or may be hidden by the peaks of other minerals. There are no obvious reflections for aluminium hydroxides. Substantial amounts of gibbsite can be ruled out on this basis, but the less well-ordered boehemite, though not indicated, would leave a weaker and thus perhaps undetectable signal.

Combining XRF and XRD to calculate mineral concentration estimates

The values shown for each mineral in Table 3 are those resulting from the calculations summarized below. The quartz XRD reflection at 26.6° 2θ correlates significantly with Si (not shown), but with the trend not passing through the origin, indicating (as expected, given the presence of kaolinite) that a mineral other than quartz also contributes to Si. This can be corrected by subtracting a factor for Al from the total Si. Using Si – 1.02*Al (the Si/Al ratio of kaolinite; Deer et al., 1966) to represent quartz, we retain a highly significant correlation with the XRD reflection ($r = 0.89$, $p < 0.0005$) as well as a slightly improved coefficient of variation and a shift of the regression line such that the intercept is indistinguishable from zero. This association between corrected Si concentration and XRD reflections confirms our quantification of quartz. Scaling the XRD data this way gives the mean and range of 14±6 wt.% for the quartz concentrations for the laterites (excluding Site 3), and 43±20 wt.% for the soils. The Site 3 laterite is excluded owing to its outlying value (53% quartz, compared with 26% for the next highest laterite).

The kaolinite XRD reflections at 12.3, 20.0, and 24.8° 2θ all correlate significantly with XRF Al concentrations, ($P<0.0005$ in all cases, $r = 0.77$, 0.79 and 0.75 respectively), and show substantial coefficients of variation (60, 62 and 56%, respectively). This confirms that kaolinite is present. However, the Al is somewhat enriched relative to kaolinite in some of the laterite samples. This is consistent with the presence of Al hydroxides, but is very uncertain. There is no direct support for this from the XRD analysis. Assuming that kaolinite comprises 20.9 wt.% Al (Deer et al., 1966), then the XRF Al concentration may be used to calculate the estimated kaolinite concentration. This yields 31±16 wt.% kaolinite for the laterite, and 13±18 for the soil. The latter is very strongly skewed by the value for the soil from Site 4 (58%); the statistics changing to 8±9 wt.% on its exclusion.

The XRD reflection at 33.2°2θ shows a very strong association with XRF Fe ($R^2 = 0.85$, with the regression line passing through the origin). This confirms that the bulk of the Fe is present in the material as either haematite or goethite, which accords well with the results shown in Formenti et al. (2014a). On the basis of comparisons between total Fe and the remaining Fe content after citrate-bicarbonate-dithionite (CBD) extraction, they show that in the Sahel dusts sampled, the mean percentage contribution of the oxides lies mostly between 64 and 68% of the total Fe. If it is assumed (for the sake of initial calculations) that all Fe is present as haematite

(haematite being 70% Fe based on ideal stoichiometry of Fe_2O_3), then the XRF Fe may be used to quantify haematite (assuming all the Fe to be present in this mineral). This would indicate 25±10 and 5±5wt.% haematite for laterite and soil respectively. Calibration of the DRS results using the transfer function derived from the calibration set in Torrent and Barron, (2002) would suggest that the haematite comprises 53-57% of the two iron oxides combined in the laterites and 43-59% in the soils. It is important to note however that these estimates are based on a transfer function derived from linear extrapolation of the regression line in Torrent and Barron (2002) well beyond the limits of the calibration data set, especially in the case of the highest calculated percentages in the laterite samples. As noted by Deaton and Balsam (1991) this may introduce significant sources of error as yet unquantified. Using Formenti et al.'s (2014b) calculated concentrations for locally derived dusts from the region, the haematite percentage would likely be closer to 35-40% of the combined oxide total. All the proposed concentrations presented in Table 3 are subject to a significant degree of uncertainty. It is also important to note that the estimated haematite concentrations in 7 out of 10 of the soils are significantly higher than those given in Balsam et al. (2014) where the values never exceed 4%.

In light of the close correlation between the XRD based values for haematite+goethite and XRF derived concentrations for total Fe noted above, it is useful to compare XRF based Fe concentrations in the 11 soil samples in the Burkina Transect considered here with those in 33 samples from the Sahel region lying to the east of the transect (Oldfield et al. 2014), but within a similar range of mean annual precipitation. The mean Fe concentration for the Burkina samples is 6.3 times higher than that from outside of the transect. Only 3 of the 33 samples have XRF values for total Fe that lie above the minimum value for the Burkina transect. A t-test on the log transformed values gives a highly significant difference, with $t = 8.84$.

Diffuse Reflectance Spectroscopy (DRS)

Table 4 summarizes the results for 8 paired laterite and soil samples from the sites located in Figure 2. Figure 9 shows the first derivative (D 1) haematite plots for the paired samples and Figure 10 shows the second derivative (D 2) haematite plots for the paired samples. For haematite, the D 1 and D 2 values are mutually consistent

(R^2= 0.98) and both show that at every site, haematite concentrations in the laterite samples are significantly higher than those in the adjacent soils. The wavelength of the D 1 peak for haematite is consistently higher for the laterite samples than for the adjacent soils (Fig. 9). This may point to mineralogical differences, e.g., a higher level of Al substitution in the soils, but the lower peak heights for the soils leave open the possibility that the shift in wavelength is related to the lower concentrations (Deaton and Balsam 1991; Balsam et al. 2014). In the case of the D 2 plots, 7 out of 8 show a shift in the wavelength of the minimum values (Fig. 10). This shift is used by Liu et al. (2011) to detect a contrast in the degree of Al substitution between lithogenic haematite in loess layers and pedogenic haematite in the intervening palaeosols. The D 1 and D 2 values for goethite are not mutually comparable, with some of the D 2 values close to the detection limit. The D 1 procedure therefore appears to be more sensitive and the values more consistent. On the basis of these, goethite values in the soils exceed those in the laterites in 6 of the 8 samples.

The aggregate XRD and DRS results for those samples used in both types of analysis are mutually consistent in showing significantly higher values for the combined iron oxides in the laterites compared with the soils. Depending on the basis of calculation using the XRD, XRF and DRS data, the laterites are between 3 and 5 times richer in haematite+goethite than the soils.

Magnetic measurements

Figure 11 shows the results of magnetic measurements of all samples from the transect. The results shown have been chosen to shed light on the extent to which our evidence supports or negates the proposition that erosion of laterite outcrops is the main process controlling the magnetic properties of the nearby soils. Whereas the majority of the paired samples have higher values in the soils for χ_{lf}, the reverse is true for SIRM. Hard IRM at both -100 mT and -300 mT, expressed as mass specific values, are, in all but one pair of adjacent samples, higher in the laterites than in the soils. The 'S' values at -100 mT and -300 mT confirm that a consistently higher percentage of SIRM remains un-reversed in these fields in the laterites than in the soils. In all but two pairs, 'Soft' IRM values are higher in the soils, as are χ_{ARM} values in all but one sample, and χ_{fd} values in seven out of the eleven pairs. χ_{fd} and χ_{ARM}/SIRM values are higher in the soils in all but three of the pairs, and χ_{ARM}/χ_{lf} in all

but two. The magnetic properties most directly reflecting the concentrations of fine, secondary ferrimagnetic grains of magnetite/maghemite formed through pedogenesis are those most strongly indicative of grains on the border between superparamagnetic (SP) and single domain (SD), with diameters around 20-25 nm, ($\chi_{fd,}$ and χ_{fd}%) and those within the narrowly defined SD range with slightly greater diameters (χ_{ARM}) (Liu et al. 2005; Oldfield et al. 2009). From the range of measurements used here, it is not possible to establish conclusively whether magnetite or maghemite is the dominant secondary ferrimagnet. Additional experiments on samples from the Sahel suggest that both magnetite and maghemite are present (Lyons et al. 2010). The values for these magnetic properties and for quotients derived from them are, with few exceptions, higher in the soils than in the laterites. The higher values for 'Hard' IRM in the laterites probably indicate a higher concentration of haematite, as is confirmed by the DRS results. In all but one pair, there is a consistent difference in the modified 'L' values (Oldfield et al. 2014), with those for the soils lower than those for the laterites. This suggests that the high field remanence in the laterites is relatively harder to reverse. This is further explored by means of the IRM acquisition experiments on three samples where the difference between the 'L' values for laterite and soil are high (Table 5; Fig. 12). All three laterite samples have three components: a ferrimagnetic component 1 with mean coercivity values ranging from 29 to 32 mT, component 2 with values between 144 and 320 mT and the largest component 3 with values between 771 and 833 mT. Only one of the soil samples (7A) has three components. In all three, component 1 dominates, with mean coercivity values ranging from 25 to 46 mT. Component 3 values lie between 650 and 811 mT. The component 2 value for sample from site 7A is 124 mT. No samples reach saturation in a DC field of 1T.

Discussion

Mineral and element comparisons from XRF and XRD.

The primary question in evaluating the data from XRF and XRD is whether or not any of the results of the element and mineral analyses preclude the possibility of the soils being derived from eroded laterite exposures with no significant subsequent geochemical modification. The XRF and XRD results are, for the most part, mutually consistent in confirming that none of the recorded differences between the soils and

laterites conclusively preclude this. Most of the differences can be explained by the more sandy nature of the soils, hence a greater abundance of quartz, relative to kaolinite, which is the dominant clay mineral in the laterites.

Particle imaging and classification

By contrast, the CCSEM analysis suggests that the soils and the laterites have different constituent particle profiles. The CCSEM classification results clearly demonstrate that the soils contain a much wider variety of particle types than the laterites. Moreover the particle assemblages in each are dominated by few specific particle types, although this is much more apparent in the laterites. The presence of Na-Al-Si-K-, Mg-Al-Si-K-Fe-, Na-Al-Si-K-Fe-, Na-Al-Si-Ca-Fe-bearing particles in the soils and their absence in the laterites is significant. The lack of these particle types in the laterite is likely the result of intensive weathering associated with laterite formation. The dominant association of Al-Si-Fe, we contend, may be due to kaolinite formation and associated Fe co-precipitation. Interestingly, Al-Si phases (likely kaolinite) are not significant in the laterite samples. We hypothesize that either any Al-Si phases in the laterites have evolved with Fe, or Al-Si formed (or was present) initially and there was subsequent Fe precipitation on this phase.

Considering the questions of the extent to which the soils have been derived from erosion of nearby laterite exposures, the CCSEM data identify a far more diverse population of particle types in the soils compared to the laterites. To go from a laterite with few particle types to a soil with many more particle types (as identified here) by a process of weathering does not seem credible. Furthermore, when the majority of the laterite particles have a specific and limited element composition (Al-Si-Fe) the likelihood that the soils have been derived entirely from erosion of nearby laterite exposures without any subsequent geochemical changes seems even less plausible.

These results also have a bearing on the extent to which the magnetic properties of the soils are derived from the laterites. Fe precipitation seems quite different in the soils as compared to the laterites. The formation of coatings appears to be in a much more advanced state in the laterites, and the presence of Fe-only particles appears to be slightly more common in the soils. Thus it would not be unreasonable to assume that the magnetic properties of the soil reflect *in situ* pedogenic processes

574 rather than inheritance from the laterites. This does not preclude the possibility that
575 there might be some, possibly windblown, contribution from the laterites to the soils;
576 high Fe content Al-Si-Fe particles that dominate in the laterites are also found in the
577 soils.

578 **Origin of soil haematite**

579 Establishing the origin of the haematite in the soils is the second of the aims set out
580 in the Introduction. For this, the most likely indicators are in the data from the DRS
581 measurements (Table 4; Figs. 9 and 10). In both the D1 (Fig. 9) and D2 (Fig. 10)
582 plots, the wavelength of the peak haematite values in almost all cases is offset
583 between the laterite and soil traces. Whereas in the former case, differences in
584 concentration cannot be precluded as a possible explanation, in the case of the D2
585 curves, Liu et al. (2011) do not consider this to be a possible explanation. The traces
586 shown here allow direct comparison with those in Liu et al. (2011; Fig. 2). In their
587 case, the plots for natural samples relate to loess and palaeosol samples from the
588 central Chinese Loess Plateau. There, the authors show a clear contrast between
589 the unweathered loess deposited during glacial intervals, reflecting a lithogenic origin
590 with minimal signs of pedogenesis, and the buried soils developed during warm,
591 moist interglacial intervals. Geochemical and magnetic analyses confirm that mature
592 soils were formed during these intervals from Miocene times onwards (Hao et al.
593 2008; Liang et al. 2009). In this case, therefore, there is a strong contrast in the
594 dominantly lithogenic haematite present in the loess and the pedogenic haematite
595 preserved in the palaeosols, for which Liu et al. (2011) infer a higher degree of Al
596 substitution. The contrast between the two is clearly revealed in the wavelength shift
597 captured by their D2 calculations. In the case of the laterite-soil comparisons
598 considered here, the haematite in both is likely to reflect formation resulting from
599 long periods of tropical weathering. Nevertheless, in all but one of the 8 pairs shown
600 in Figure 10, there is a variable, but detectable shift. Whether the shift reflects
601 greater Al substitution in the soils, or some other difference, for example in grain size
602 or matrix, is not possible to resolve conclusively from the present evidence. The soils
603 are, on average, less rich in Al than the laterites. Moreover, the deconvolution of the
604 IRM acquisition curves (Table 5; Fig. 12) identifies a medium coercivity component
605 (Component 2) that may be Al-substituted haematite in all three laterite samples, but
606 in only one of the soil samples (see below).

607 Irrespective of the reason for the wavelength shift in the second derivative of the
608 DRS spectra, we take it to indicate either that the haematite in the laterites and soils
609 has developed independently in the two as a result of differences in the weathering
610 processes experienced, or that any haematite transferred to the soils from the
611 nearby laterites has been modified by further weathering in the soils under the
612 climatic and pedogenic conditions prevailing subsequent to any erosive transfer. The
613 latter interpretation is consistent with the eroded nature of the laterite outcrops close
614 to the sites providing the soil samples (Fig. 1). Also strongly favouring the latter
615 interpretation is the much higher total iron content in the soils in the transect
616 compared with that in soils from the Sahel lying further to the east, within a region
617 experiencing similar precipitation values, but not adjacent to laterite outcrops (see
618 above).

619 **Origin of the magnetic properties**

620 In most earlier papers comparing the magnetic properties of soils with those of
621 substrates, the comparison was with material derived from unweathered bedrock
622 (Oldfield et al. 1979; Walling et al. 1979). In the present case, the comparison is
623 complicated by the fact that the putative source of the soils is highly weathered
624 material. The most consistent differences between the laterites and soils confirm that
625 the latter are richer in ferrimagnetic minerals, especially grains of stable single
626 domain (SD) or finer sizes. The results of the IRM acquisition experiments (Table 5;
627 Fig. 12) strongly reinforce this observation. These findings are consistent with the
628 neo-formation of pedogenic magnetite/maghemite during weathering and soil
629 formation, irrespective of the original source of the iron present. The consistently
630 higher HIRM-100 and HIRM-300 values as well as the consistently 'harder' 'S' values
631 in the laterites are consistent with the higher haematite concentrations indicated by
632 the DRS analyses. The differences in modified 'L' values noted above are less easy
633 to interpret in terms of magnetic mineralogy. Hu et al. (2013) and Liu et al. (2015)
634 identify marked differences in the coercivity of IRM and the DRS spectra in
635 haematite on the basis of the degree of aluminium substitution. They show that in
636 the Chinese palaeosol-loess sequences they analyzed, low coercivity-high Al
637 substituted haematite is a significant pedogenic component alongside lithogenic
638 haematite with a much higher coercivity. It is likely that component 2 in the IRM
639 acquisition results reflects Al substituted haematite and its presence in all three

laterite samples analysed (Fig. 12; Table 5) is not surprising. It is also detectable in one of the three soil samples. These results suggest that there is no single, simple explanation for the differences in modified 'L' values shown in Figure 11. Overall, the magnetic properties confirm a much higher fine-grained ferrimagnetic (magnetite/maghemite) and lower antiferromagnetic (dominantly haematite) contribution in the soils. The enrichment in fine grained ferrimagnets points to pedogenic enhancement leading to the neo-formation of secondary magnetite/maghemite, as has been inferred from previous studies of Sahel soils (Lyons et al. 2010; 2012; Balsam et al. 2011; Oldfield et al. 2014).

Conclusions

The mineral and element analyses provided by XRF and XRD analysis do not preclude the possibility that eroding laterite exposures nearby have made a major contribution to the geochemical properties of nearby soils, nor do they preclude the alternative view that the soils have evolved independently. Most of the differences in element and mineral constituents and proportions that they demonstrate can be explained by changes generated by different concentrations of aluminium and quartz, selective winnowing of fine soils particles and eluviation, the process leading to enrichment in the clay fraction at depths below those sampled and thus contributing to the relatively coarse grained, quartz-rich nature of the surface soils. The link between higher iron concentrations and proximity to eroding laterite outcrops noted above does however support the view that the laterites have had a strong influence at least on the total iron content of the soils.

Particle imaging and characterization by CCSEM and EDS provide conclusive evidence that, despite their proximity to outcrops of eroding laterite, the soils and their constituent particles were not derived exclusively from the laterites. Although the greater range of mineral classes in the soils might be interpreted as a result of aeolian inputs, the contrasts in particles within the same class shown in Figures 7 and 8 are indicative of differences in origin and formation consistent with soil development independent of any inputs from the laterites. The magnetic measurements confirm that several indicative magnetic properties of the soils, notably enrichment in fine-grained ferrimagnets and lower haematite content

671 compared with the laterites, reflect the effects of pedogenesis subsequent to and
672 irrespective of any possible derivation from the laterites.

673 Turning to the hypotheses considered at the outset, the evidence as a whole
674 therefore precludes either of the two simplest and opposed hypotheses, namely that
675 the soils reflect recent erosion from the existing laterite exposures with no
676 subsequent geochemical transformation, or that the composition of the soils reflects
677 weathering and pedogenesis entirely uninfluenced by proximity to the laterite
678 outcrops. We conclude that the relationship between the laterites and soils is more
679 complex. The results from XRF and XRD analyses, especially the evidence that
680 total iron concentrations in the soils across the transect are, on average, over 6
681 times those in soils less closely associated with eroding laterites, suggest that the
682 development of the soils was not entirely uninfluenced by their proximity to the
683 laterite outcrops. The evidence from the CCSEM, EDS, DRS and magnetic
684 measurements, however, indicates that during the time elapsed since any material
685 eroded from the laterite outcrops contributed to the formation of the soils or to the
686 substrates upon which they developed, the subsequent passage of time has been
687 sufficient to allow the development or incorporation of particle classes not found in
688 the laterites and also modification of the haematite present in the soils, as well as
689 their magnetic properties. The laterites appear to have been formed at least 24
690 million years ago (Gunnell 2003) with little evidence for subsequent geochemical
691 transformation. This long time interval has been sufficient for their erosion and the
692 subsequent modification of the soils derived in part from that process, as well as for
693 both weathering of the parent material underlying the soils and surface processes at
694 the soil-atmosphere interface involving both deflation and deposition. We infer that in
695 conjunction, these processes have led to the characteristics that have given the soils
696 distinctive particle assemblages, iron oxide geochemistry and magnetic properties.

697 The magnetic measurements presented here provide no support for the view that
698 eroding laterites are responsible for the poor correlation between rainfall and soil
699 magnetic properties along the transect reported in Oldfield et al. (2014), compared
700 with the results summarised in Lyons et al. (2010), where a strong correlation was
701 indicated. A more likely explanation lies in the greater spread of rainfall values
702 across the transects considered by Lyons et al. (2010). In that case, rainfall values

range from <5 to >1300 mm p.a. In the later study, no values exceed 1000 mm p.a. and over 50% of the sites lie between the 200 and 600 mm p.a. isohyets.

On this basis, the extent to which the red coloration and distinctive reflectance characteristics of the soils have been strongly influenced by erosion of laterite exposures remains an open question, since the DRS analyses include evidence that the haematite in the soils has resulted, in part at least, through *in situ* weathering and pedogenesis. The present evidence provides no clear indication of the relative importance of these two interacting processes. None of the evidence presented counters the inference of a climate-soil magnetic susceptibility link inferred from previous research across the Sahel and Sahara transition.

Acknowledgements

We thank Henry Francis, Kentucky Geological Survey at the University of Kentucky, Lexington KY and Professor Asish Basu and the UTA Shimadzu Center for Environmental, Forensics, and Material Science for contributing the XRD analyses summarized in Table 3, Mike O'Connor and Jennifer Mobbs for many of the magnetic measurements, Zachary Sutton for CCSEM results, Danielle Alderson for the DRS and XRF measurements and Suzanne Yee for help with the Figures.

References

Aleva Gjj (compiler). 1994. *Laterites. Concepts, geology, morphology and chemistry.* ISRIC, Wageningen. 175pp.

Arimoto R, Balsam W, Schloesslin C. 2002. Visible spectroscopy of aerosol particles collected on filters: iron-oxide minerals. *Atmospheric Environment* **36**: 89-96.

Balsam WL, Ellwood BB, Ji J, Williams ER, Long X, El Hassani A. 2011. Magnetic susceptibility as a proxy for rainfall: Worldwide data from tropical and temperate climate. *Quaternary Science Reviews* **30**: 2732-2744.

730 Balsam W, Ji J, Renock D, Deaton BC, Williams E. 2014. Determining haematite
731 content from NUV/Vis/NIR spectra: limits of detection. *American Mineralogist* **99,**
732 2280-2291.

733 Burke K, Gunnell Y. 2008 .The African Erosion Surface: A Continental-scale
734 Synthesis of Geomorphology, Tectonics, and Environmental Change over the Past
735 180 Million Years. Geological Society of America: Memoir 201 p.1-66. ISBN-13: 978-
736 0-8137-1201-7

737 Deaton BC, Balsam WL. 1991. Visible spectroscopy - a rapid method for determining
738 haematite and goethite concentration in geological materials. *Journal of Sedimentary*
739 *Petrology* **61**: 628 – 632.
740 Deckers JA, Nachtergaele F, Spaargaren OC. (Eds.) (1998). World Reference Base
741 for Soil Resources: Introduction. International Society of Soil Science, Leuven,
742 Belgium. Pp. 100-107.

743 Deer WA, Howie RA, Zussman J. 1966. *An introduction to the rock forming minerals.*
744 Longman, London, 528pp.

745 Eberl DD. 2003. *User's guide to RockJock -- A program for determining quantitative*
746 *mineralogy from powder X-ray diffraction data*: U.S. Geological Survey Open-File
747 Report 2003-78, 47 p.

748 FAO. 2006. World reference base for soil resources. *World Soil Resources*
749 *Report 103*. Rome: Food and Agriculture Organization of the United Nations,
750 132 pp.

751

752 Formenti P, Caquineau S, Chavaillier S, Klaver AK, Rajot JL, Belin S, Briois V. 2014
753 (a) Dominance of goethite over hematite in iron oxides of mineral dust from western
754 Africa: quantitative partitioning by X-ray Absorption spectroscopy. *Journal of*
755 *Geophysical Research Atmospheres* 119, 12740-12754.
756

757 Formenti P, Caquineau S, Desbouefs S, Chavaillier S, Klaver A, Chavaillier, Journet
758 SK, Rajot JL. 2014(b) Mapping the physico-chemical properties of mineral dust in
759 western Africa: mineralogical composition. *Atmospheric Chemistry and Physics,* **14**,
760 10663-10686.

Goldstein J, Newbury DE, Joy DC, Lyman CE, Echlin P, Lifshin E, Sawyer L, Michael JR. 2003. *Scanning Electron Microscopy and X-ray Microanalysis*. New York: Springer Science Third Edition p. 75.

Grey W, North PRJ, Sietse Los O. 2005. Retrieving Aerosol properties and Land Surface Albedo over the Sahel from AATSR Observations*. Proceedings of the 2004 Envisat & ERS Symposium (ESA SP-572)*. 6-10 September 2004, Salzburg, Austria. Edited by H. Lacoste and L. Ouwehand. Published on CD-Rom., #285.1

Gunnell Y. 2003. Radiometric ages of laterites and constraints on long-term denudation rates in West Africa. *Geology* **31**: 1v31-134

Hao Q, Oldfield F, Bloemendal J, Guo Z. 2008. The magnetic properties of loess and palaeosol samples from the Chinese Loess Plateau spanning the last 22 million years. *Palaeogeography, Palaeoclimatology, Palaeoecology* **260**: 389-404.

Heslop D, Dekkers MJ, Kruiver PP, van Oorschot HM. 2002. Analysis of isothermal remanent magnetization acquisition curves using the expectation-maximization algorithm. *Geophysical Journal International* **148**: 58-64.

Hu P, Liu Q, Torrent J, Barrón V, Jin C. 2013. Characterizing and quantifying iron oxides in Chinese loess/paleosols: Implications for pedogenesis. *Earth and Planetary Science Letters* 10/2013; 369–370:271–283. DOI:10.1016/j.epsl.2013.03.033.

Liang M, Guo Z, Kahmann JA, Gu Z, Oldfield F. 2009. Geochemical characteristics of the Miocene eolian deposits in China: the provenance and climate implications *Geochemistry Geophysics Geosystems* 10, 16pp. Q04004, doi:10.1029/2008GC002331

Liu Q, Torrent J, Maher BA, Yu Y, Deng C, Zhu R, Zhao X. 2005. Quantifying grain size distribution of pedogenic magnetic particles in Chinese loess and its significance for pedogenesis. *Journal of Geophysical Research* 110, B11102, DOI: 10.1029/2005JB003726.

Liu Q, Sun Y, Qiang X, Tada R, Hu P, Duan Z, Jiang Z, Liu J, Su K. 2015. Characterizing magnetic mineral assemblages of surface sediments from major Asian dust sources and implications for the Chinese loess magnetism. *Earth Planets and Space* 05/2015; 67(1). DOI:10.1186/s40623-015-0237-8.

Liu QS, Torrent J, Barron V, Duan ZQ, Bloemendal J. 2011. Quantification of hematite from the visible diffuse reflectance spectrum: effects of aluminium substitution and grain morphology. *Clay Minerals* **46**: 137-147.

Lyons R, Oldfield F, Williams E. 2010. Mineral magnetic properties of surface soils and sands across four North African transects and links to climatic gradients. *Geochemistry, Geophysics, Geosystems* 11, Q08023. doi:10.1029/2010GC003183.

Lyons R, Oldfield F, Williams E. 2012. The possible role of magnetic measurements in the discrimination of Sahara/Sahel dust sources. *Earth Surface Processes and Landforms* **37**: 594-606.

Maher BA. 2011. The magnetic properties of Quaternary aeolian dusts and sediments, and their palaeoclimatic significance. *Aeolian Research* **3**: 87-145.

Maher BA, Thompson R. 1992. Palaeoclimatic significance of the mineral magnetic record of Chinese loess and palaeosols. *Quaternary Research* **37**: 155–170.

Maher BA, Possolo A. 2013. Statistical models for use of palaeosol magnetic properties as proxies of palaeorainfall. *Global and Planetary Change* **111**: 280-287.

Oldfield F, Rummery TA, Thompson R, Walling DE. 1979. Identification of suspended sediment sources by means of magnetic measurements – some preliminary results. *Water Resources Research* **15**: 211–18.

Oldfield F, Hao Q, Bloemendal J, Gibbs-Eggar Z, Patil S, Guo Z. 2009. Links between bulk sediment particle size and magnetic grain-size: general observations and implications for Chinese loess studies. *Sedimentology* doi: 10.1111/j.1365-3091.2009.01071.x

822 Oldfield F. 2012. Mud and magnetism: records of late Pleistocene and Holocene
823 environmental change recorded by magnetic measurements. *Journal of*
824 *Paleolimnology*. doi: 10.1007/s10933-012-9648-8.

825 Oldfield F, Chiverrell RC, Lyons R, Williams E, Shen Z, Bristow C, Bloemendal J,
826 Torrent J, Boyle JF. 2014. Discriminating dusts and dusts sources using magnetic
827 properties and haematite:goethite ratios of surface materials and dust from North
828 Africa, the Atlantic and Barbados. *Aeolian Research* **13**: 91-104.

829 Schaaf C, personal communication, 2009

830 Scheinost AC, Chavernas A, Barrón V, Torrent J. 1998. Use and limitations of the
831 second-derivative diffuse reflectance spectroscopy in the visible to near-infrared
832 range to identify and quantify Fe oxide minerals in soils. *Clays and Clay Minerals* **46**:
833 528−536.

834 Schellmann W. 2008. An Introduction to Laterite: Products and processes of
835 intensive rock weathering http://www.laterite.de/

836 Tardy Y, Kobilsex B, Paquet H. 1991. Mineralogical composition and geographical
837 distribution of African and Brazilian periatlantic laterites. The influence of continental
838 drift and tropical paleoclimates during the past 150 million years and implications for
839 India and Australia
840 *Journal of African Earth Sciences* **12**: 283-295.

841 Tardy Y, Boeglin J-L, Novikoff A, Roquin C. 1995. Petrological and geochemical
842 classification of laterites. Proceedings of the 10th International Clay **:** Adelaide,
843 Australia, July 18 to 23, 1993 CSIRO 1 Melbourne 1995.

844 Torrent J, Barrón V, 2002. Diffuse reflectance spectroscopy of iron oxides. In
845 Hubbard AT. (Ed.) *Encyclopedia of Surface and Colloid Science*, Taylor and Francis,
846 New York, pp. 1438 – 1446.

847 Torrent J, Liu Q, Bloemendal J, Barrón V. 2007. Magnetic Enhancement and Iron
848 oxides in the Upper Luochuan Loess-Paleosol Sequence, Chinese Loess Plateau.
849 *Soil Science Society of America Journal* **71**: 1570 – 1578.

850 Walden J, Oldfield F, Smith J. (Eds). 1999. *Environmental magnetism: a practical*

guide. Quaternary Research Association Technical Guide.

Walling DE, Peart MR, Oldfield F, Thompson R. 1979. Suspended sediment sources identified by magnetic measurements. *Nature* **281**: 110–13.

Widdowson M. 2007. Laterite and Ferricrete. In: Nash D J, McLaren S J. (Eds.) *Geochemical Sediments and Landscapes*. Oxford, UK: Wiley-Blackwell, pp. 46–94.

Williams EW, Balsam W, Schaaf C, Yang X, Zhang Q, Ji J, Thorncroft C, Hicks E. 2009. Iron Oxide Control on the Surface Albedo of West Africa, Third AMMA Workshop, Ouagadougou, Burkina Faso, July 20-24, 2009.

World Soil Information (International Soil Research Information Centre). www.isric.org/isric/webdocs/docs/major_soils_of_the_world/set6/lx/lixisol.pdf

Zhou LP, Oldfield F, Wintle AG, Robinson SG, Wang JT. 1990. Partly pedogenic origin of magnetic variations in Chinese loess. *Nature* **346**: 737–39.

Table 1. Class assignments (% total) for individual particles (data collected by CCSEM) for Burkina soils (see section 4.2).

		Burkina soil 4A	**Burkina soil 5A**	**Burkina soil 6A**	**Burkina soil 7A**	**Burkina soil 10A**	**Burkina soil 11A**	**Burkina soil** 12A
		n = 3,240	*n* = 2,925	*n* = 5,194	*n* = 3,132	*n* = 2,061	*n* = 4,502	*n* = 5,767
Class	**Class description**							
1	Si-only	2.3	5.9	9.2	2.3	1.9	1.8	8.3
3	Fe-only	1.5	2.1		1.4		2.9	
6	Ti-rich						2.5	
8	Al-Si-only	26.1	5.6	17.3	5.5	9.6	5.6	16.2
17	Si-Fe-only				1.0		1.1	
30	Al-Si-Fe-only	48.7	51.2	43.6	43.6	51.5	58.1	52.6
31	Al-Si-K-only	4.0	2.7	5.5	5.0	1.0		4.5
33	Na-Al-Si-only				1.8			

35	Na-Al-Si-Fe-only		4.4	2.1	7.8	14.3	1.1	
36	Na-Al-Si-K-only			1.0		1.0		0.6
37	Al-Si-K-Fe-only	5.9	7.3	4.9	6.5	3.8	11.4	5.0
38	Mg-Al-Si-Fe-only		1.1				1.8	
39	Al-Si-Fe-P-only						4.6	
47	Mg-Al-Si-K-Fe-only		2.7		2.9	1.3	1.0	0.8
49	Na-Al-Si-Ca-Fe-only			1.4		1.7		
51	Na-Al-Si-K-Fe-only		1.5		2.5	1.7	1.0	1.0
57	Low Ti	3.8	4.1	9.0	6.3	3.4		3.3
58	Mn-bearing				2.0	1.3		0.6
100	Other	1.5	3.6		6.1	1.0	6.9	4.0

Table 2. Class assignments (% total) for individual particles (data collected by CCSEM) for Burkina laterites (see section 4.2).

		Burkina lat. 0	**Burkina lat. 1**	**Burkina lat. 3**	**Burkina lat. 4**	**Burkina lat. 5**	**Burkina lat. 7**	**Burkina lat. 8**	**Burkina lat. 9**	**Burkina lat. 10**
		n = 6,713	*n* = 6,063	*n* = 6,944	*n* = 4,503	*n* = 2,061	*n* = 3,140	*n* = 3,998	*n* = 6,245	*n* = 3,422
Class	**Class description**									
1	Si-only	0.4		3.9				1.0		
3	Fe-only	9.4			1.3					1.9
8	Al-Si-only		2.0	14.7				8.6		
17	Si-Fe-only	11.7								
30	Al-Si-Fe-only	56.0	90.9	54.5	83.2	78.2	72.5	70.1	87.5	
31	Al-Si-K-only			2.0				2.5		
34	Na-Al-Si-Ca-only							1.0		

35	Na-Al-Si-Fe-only	0.6		3.1	1.2		8.5	0.7	1.4	
37	Al-Si-K-Fe-only	15.8	0.8	6.8	7.1	7.6	7.1	3.9	3.6	6.3
40	Al-Si-Fe-P-only	1.4								
49	Na-Al-Si-Ca-Fe-only	0.7			1.0					
57	Low Ti		4.2			10.3	2.3	3.4	0.8	1.5
58	Mn-bearing						1.5			
100	Other	1.3						4.0	2.1	

Table 3. X-Ray Diffraction data for laterites and soil samples The values shown are percentage contributions of each mineral to the total mineral content in each sample calculated as described in Section 4.4. The values for Haematite+Goethite are estimates subject to the caveats outlined in the text.

Site	Quartz		Kaolinite		Haematite + Goethite		Illite	
	Laterite	Soil	Laterite	Soil	Laterite	Soil	Laterite	Soil
1	12	61	47	0	24	5	-	-
3	53	49	43	3	7	2	++	-
4	11	10	11	58	34	18	+	-
5	10	35	53	1	27	4	+	-
6	12	13	20	3	30	2	-	+
7	11	70	15	9	19	0	-	-
8	24	62	38	10	12	5		
9	13	39	45	27	25	5		
10	10	46	18	6	35	5		
11	26	47	17	17	39	8		

Table 4. DRS results for paired laterite and soil samples from 8 sites located in Figure 2.

D1 – First Derivative of percentage reflectance (Balsam et al. 2014), (Deaton et al. 1991);

D 2 – Second Derivative of percentage reflectance (Scheinhorst et al. 1998; Torrent and Barron 2002; Torrent et al. (2007). Hm – Haematite; Gt – Goethite

Site	D1	D1	D2	D2	D1	D1	D2	D2	D2	D2
	Hm	Hm	Hm	Hm	Gt	Gt	Gt	GT	Hm/Hm+Gt	Hm/Hm+Gt
	Peak height	Peak height	Peak amplitude	Peak amplitude	Peak height	Peak height	Peak amplitude	Peak amplitude		
1/1A	427	158	70	20	89	92	17	10	0.80	0.68
3/3A	635	257	104	34	111	152	16	21	0.87	0.62
4/4A	234	96	40	18	58	34	10	1	0.80	0.93
5/5A	407	115	69	19	32	45	9	2	0.89	0.92
7/7A	302	135	48	19	55	71	9	4	0.84	0.82
8/8A	386	98	62	15	50	66	8	1	0.89	0.91
9/9A	377	240	67	35	67	46	11	6	0.86	0.86
10/10A	337	269	56	39	59	82	11	9	0.84	0.81
	LAT	SOIL	LAT	SOIL	LAT	SOIL	LAT	SOIL	LAT	SOIL

Table 5. Acquisition of IRM - deconvolution results.

$B_{1/2}$ represents the applied field at which the mineral phase represented acquires half of its saturation IRM, i.e. the mean coercivity of that part of the IRM acquisition spectrum. The dispersion parameter (DP) represents one standard deviation of the log-normal distribution for each magnetic mineral component, thus expressing its coercivity distribution. The parameter 'Relative contribution' records the contribution each component makes to the total IRM acquisition up to 1T. The $B_{1/2}$ values are derived from the succession of peaks in the IRM acquisition diagrams (Fig. 10). Components with a $B_{1/2}$ value of less than 70 mT are likely to reflect the contribution from ferrimagnetic minerals (magnetite/maghemite), and those with $B_{1/2}$ values above 100 mT are likely to reflect the contributions from imperfect anti-ferromagnetic minerals (haematite and, to a lesser extent, goethite).

Sample	Component 1			Component 2			Component 3		
	$B_{1/2}$ (mT)	DP (mT)	Relative contribution	$B_{1/2}$ (mT)	DP (mT)	Relative contribution	$B_{1/2}$ (mT)	DP (mT)	Relative contribution
7 Laterite	32	2	0.13	420	2	0.15	771	2	0.72
8 Laterite	29	2	0.37	144	3	0.19	800	2	0.44
11 Laterite	30	2	0.12	375	2	0.15	833	2	0.72
7A Soil	29	2	0.49	124	2	0.24	710	2	0.27
8A Soil	46	3	0.73				650	5	0.27
11 A Soil	25	2	0.58				811	2	0.42

Figure captions

Figure 1. Typical eroding laterite exposure and adjacent soil colored by haematite.

Figure 2. Location map showing the sites sampled on the transect.

Figure 3. Proportion Diagrams of selected elements determined by X-Ray Fluorescence.

Figure 4. Scanning electron micrographs of Al-Si (a), Na-Al-Si-K (b), Mg-Al-Si-K-Fe (c), Na-Al-Si-K-Fe (d) -bearing particles from soil 6

Figure 5. Scanning electron micrographs of Fe particles from soil 11 (a and b), and Fe particles from laterite 0 (c and d)

Figure 6a. Ternary plot for the Al, Si and Fe concentrations for particles assigned to class 30 from the CCSEM analysis of soil site 6 (n = 2,263 particles)

Figure 6b. Ternary plot for the Al, Si and Fe concentrations for particles assigned to class 30 from the CCSEM analysis of laterite site 0 (n = 3,760 particles)

Figure 7. Scanning electron micrographs of Al-Si-Fe-only-bearing particles from soil 10 (a.-d.)

Figure 8. Scanning electron micrographs of Al-Si-Fe-only-bearing particles from laterite 10 (a.-d.)

Figure 9. DRS. First Derivative results (D 1), for haematite in paired laterites and soils at eight sites. Site locations shown on Figure 2.

Figure 10. DRS. Secod Derivative (D 2) results for haematite in paired laterites and soils at eight sites. Vertical lines pass through the minimum wavelength for each sample. Site locations shown on Figure 2.

Figure 11. Results of magnetic measurements of all 14 samples (0 – 13) from the transect

Figure 12. IRM acquisition – de-convolution plots for 3 paired laterite and soil samples from sites 7, 8 and 11.

Figure 1. Typical eroding laterite exposure and adjacent soil

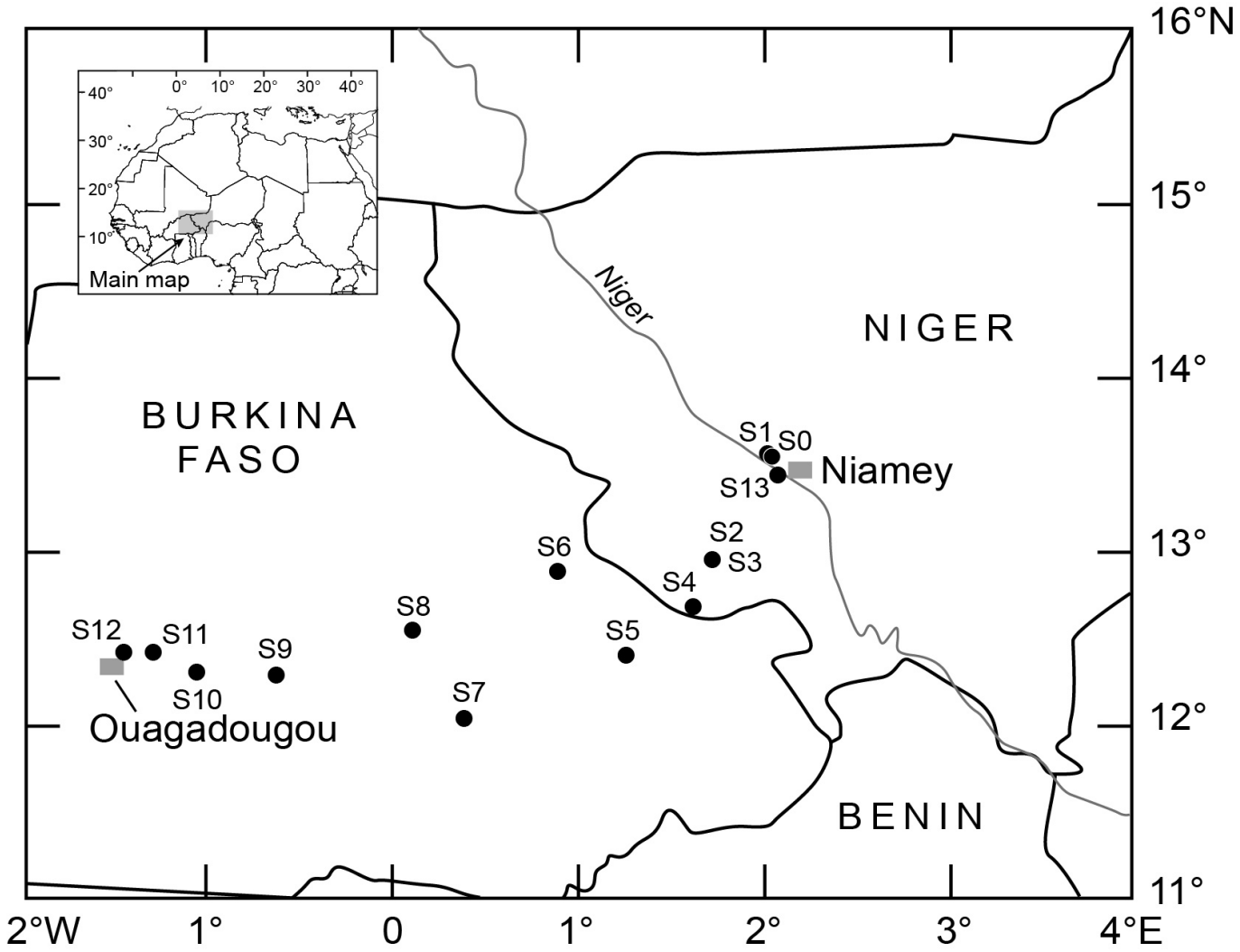

Figure 2. Location map showing the sites sampled on the transect.

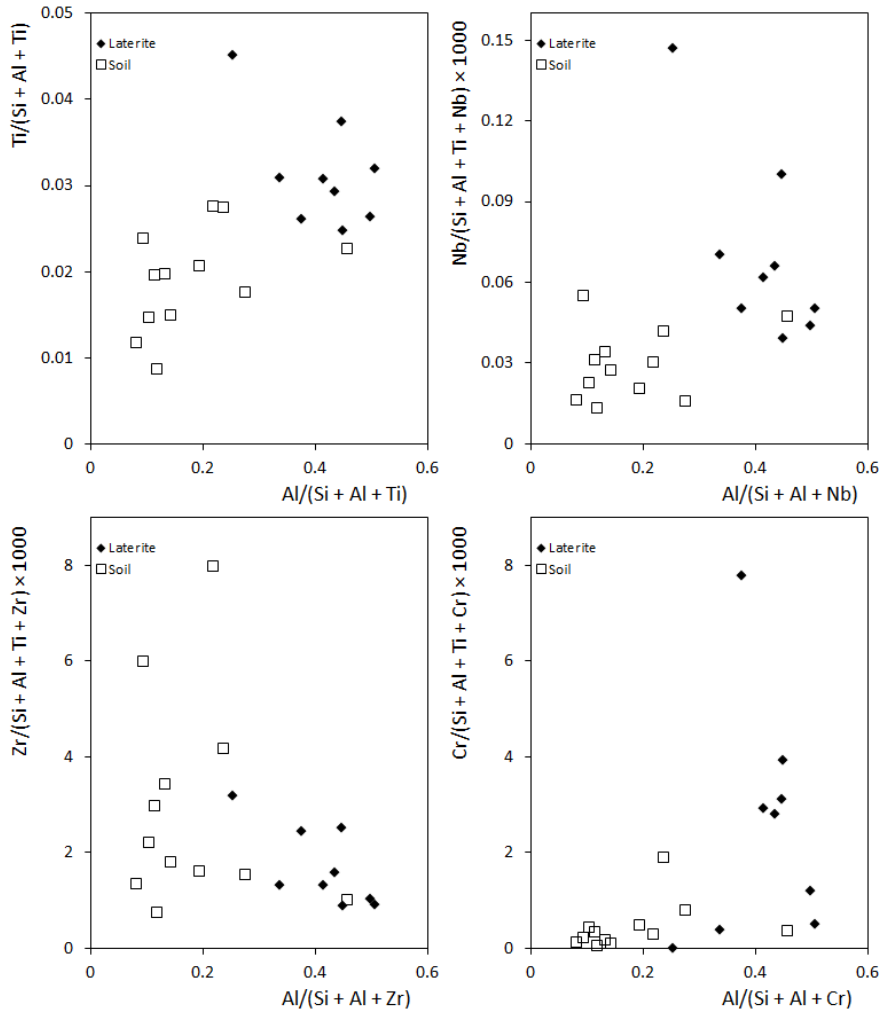

Figure 3. Proportion Diagrams of selected elements determined by XRF.

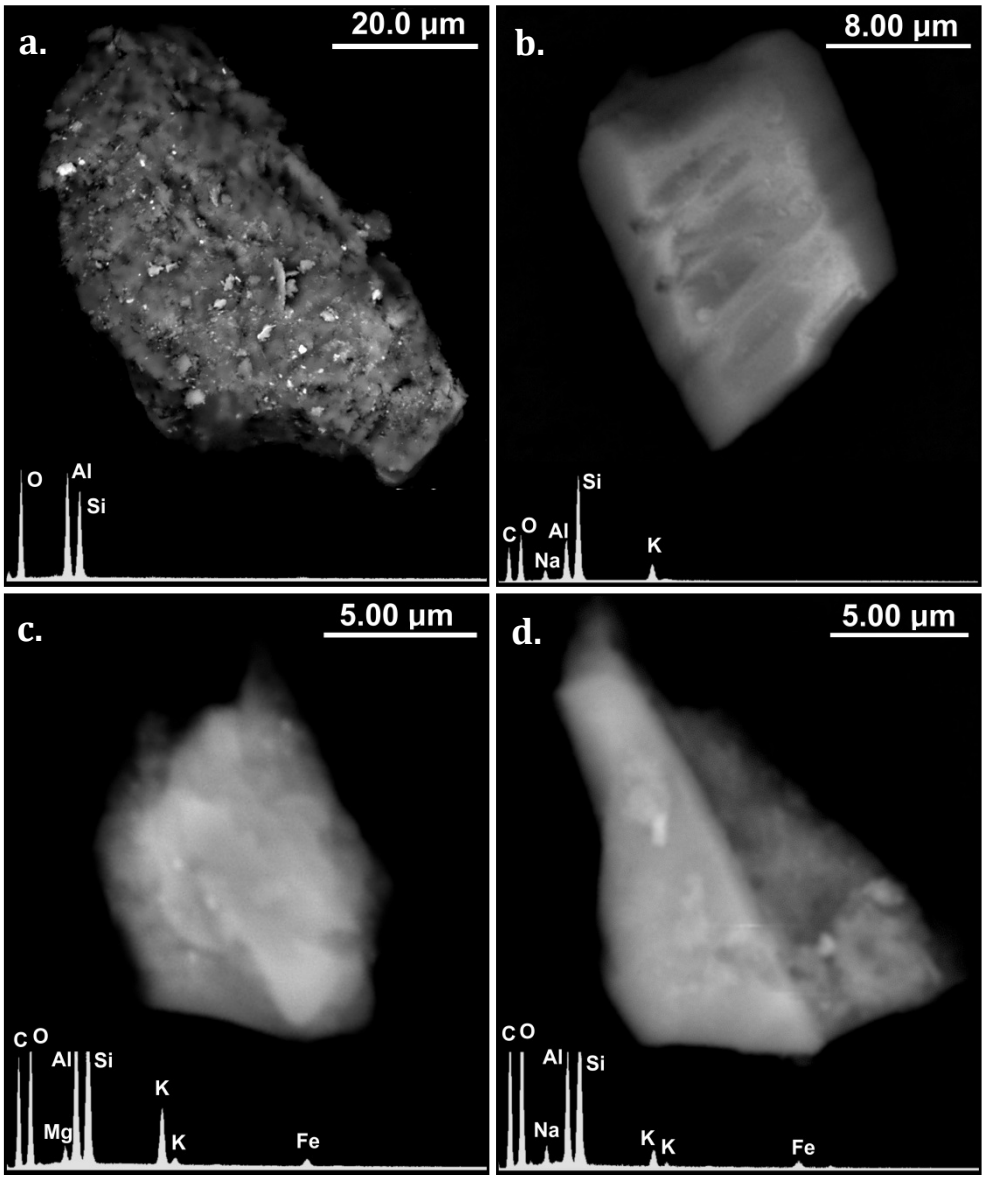

Figure 4. Scanning electron micrographs of Al-Si (a), Na-Al-Si-K (b), Mg-Al-Si-K-Fe (c), Na-Al-Si-K-Fe (d) -bearing particles from soil 6A. Site locations shown on Figure 2.

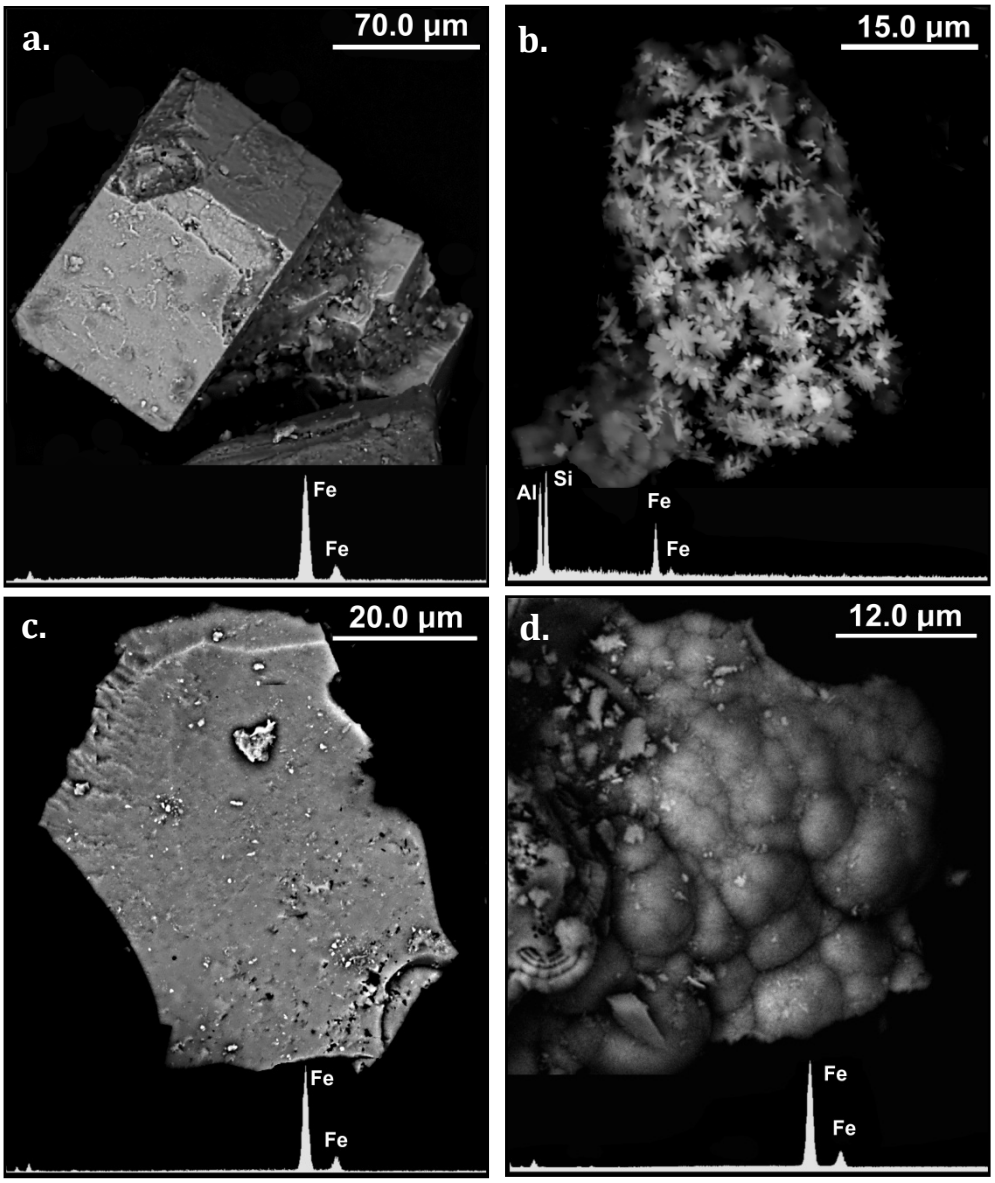

Figure 5. Scanning electron micrographs of Fe particles from soil 11A (a and b), and Fe particles from laterite 0 (c and d). Site locations shown on Figure 2.

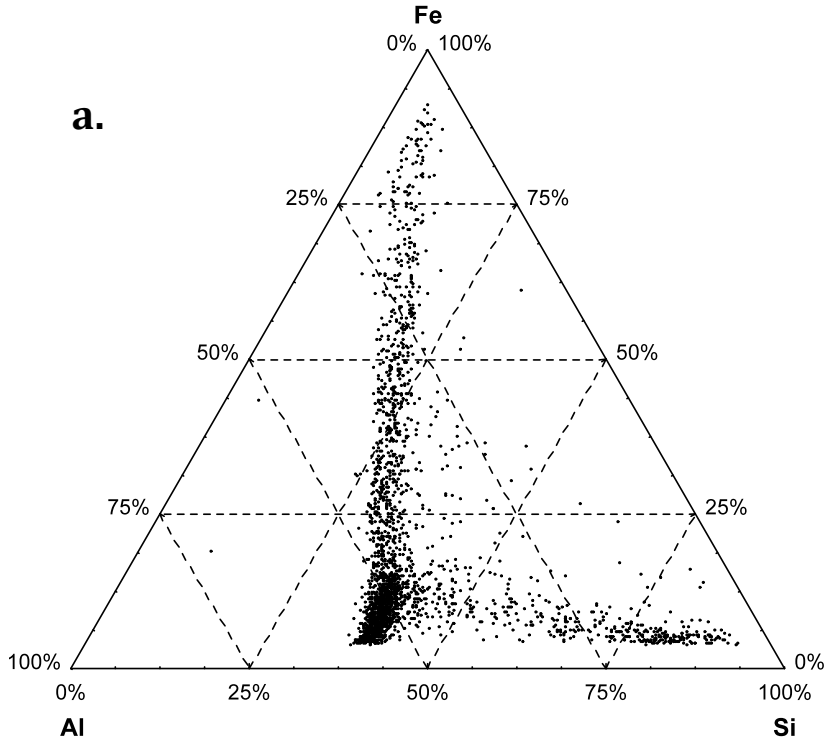

Figure 6a. Ternary plot for the Al, Si and Fe concentrations for particles assigned to class 30 from the CCSEM analysis of soil site 6 (n = 2,263 particles)

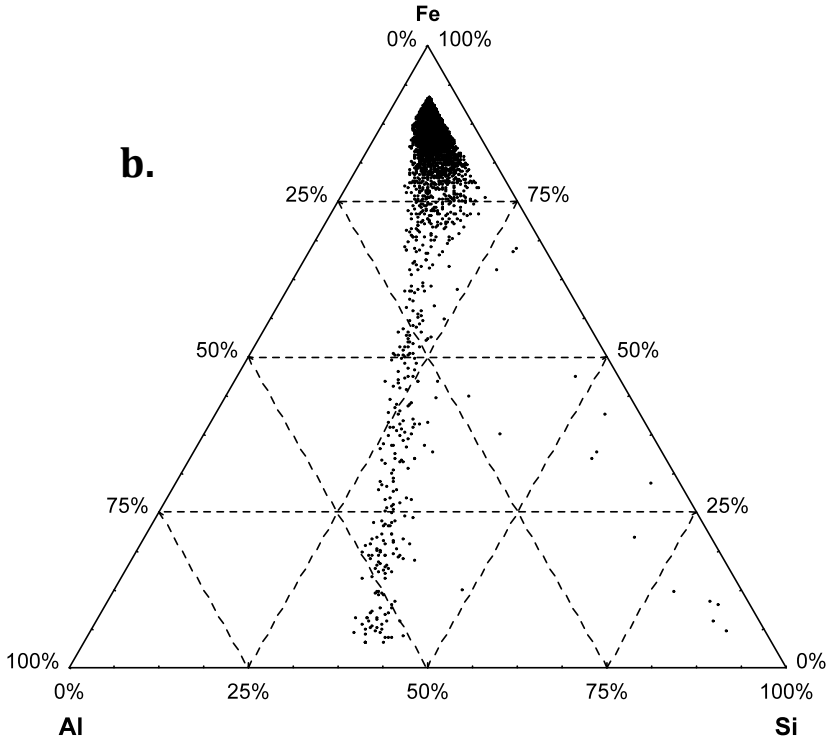

Figure 6b. Ternary plot for the Al, Si and Fe concentrations for particles assigned to class 30 from the CCSEM analysis of laterite site 0 (n = 3,760 particles)

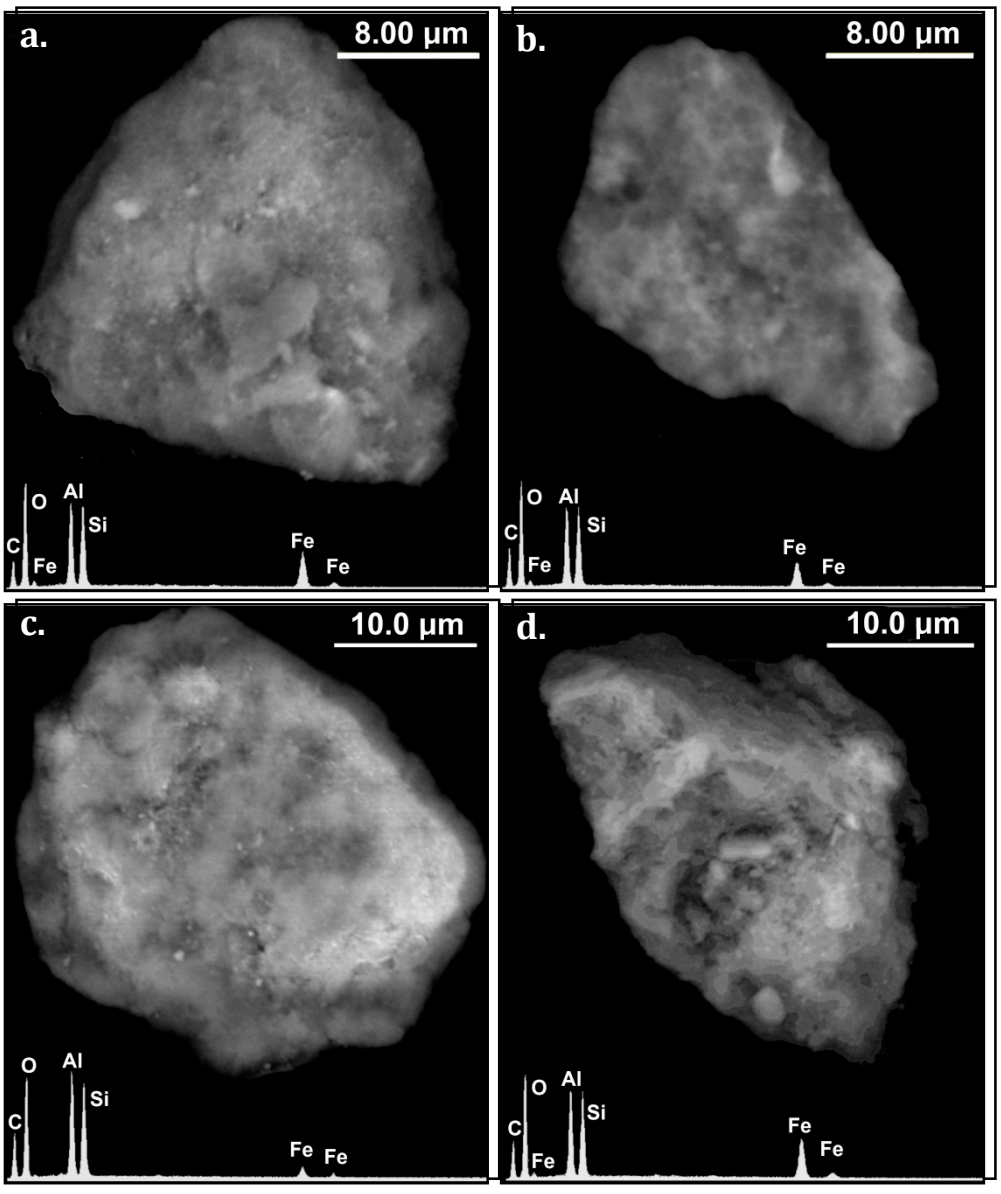

Figure 7. Scanning electron micrographs of Al-Si-Fe-only-bearing particles from soil 10A (a-d.). Site locations shown on Figure 2.

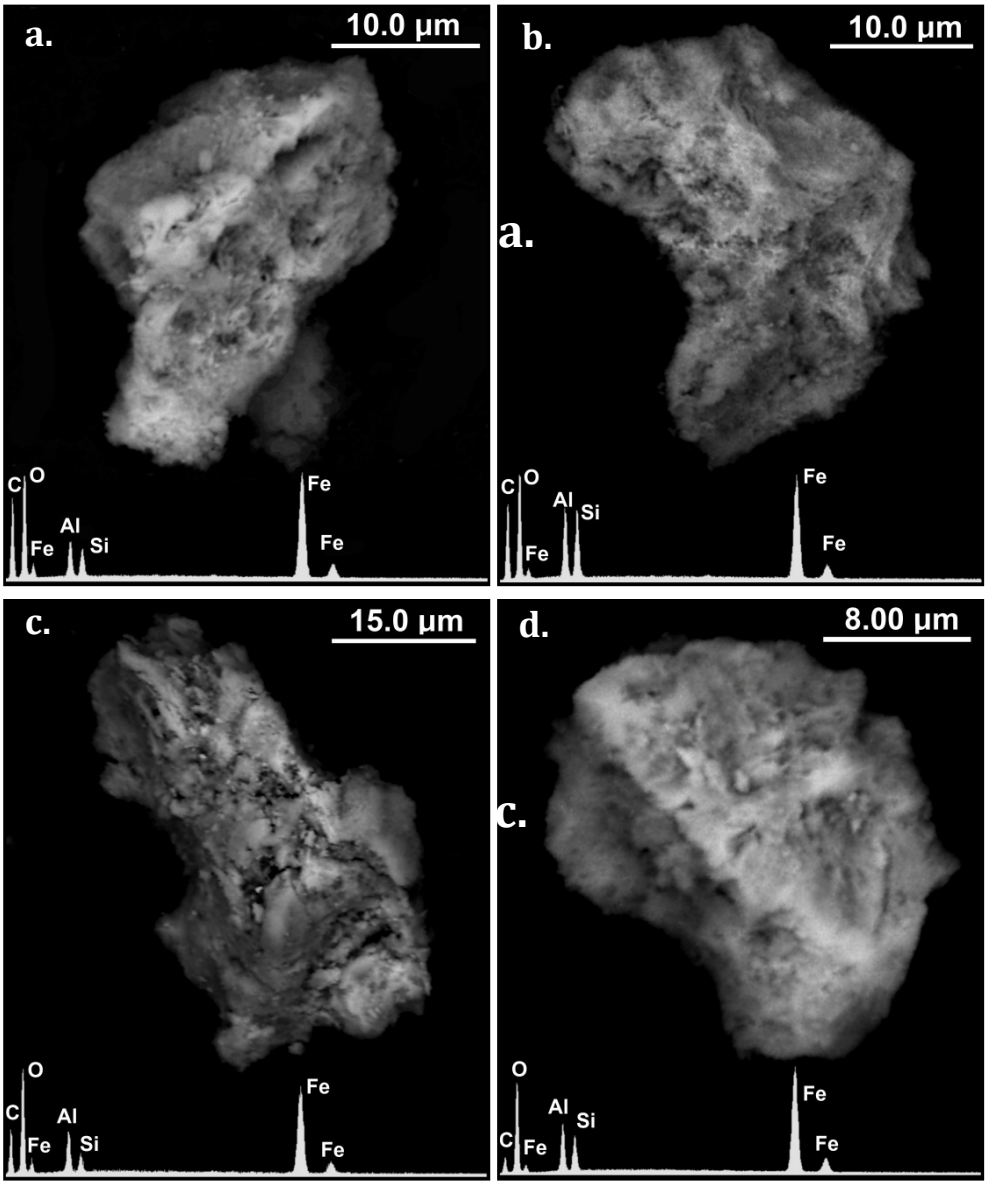

Figure 8. Scanning electron micrographs of Al-Si-Fe-only-bearing particles from laterite 10 (a.-d). Site locations shown on Figure 2.

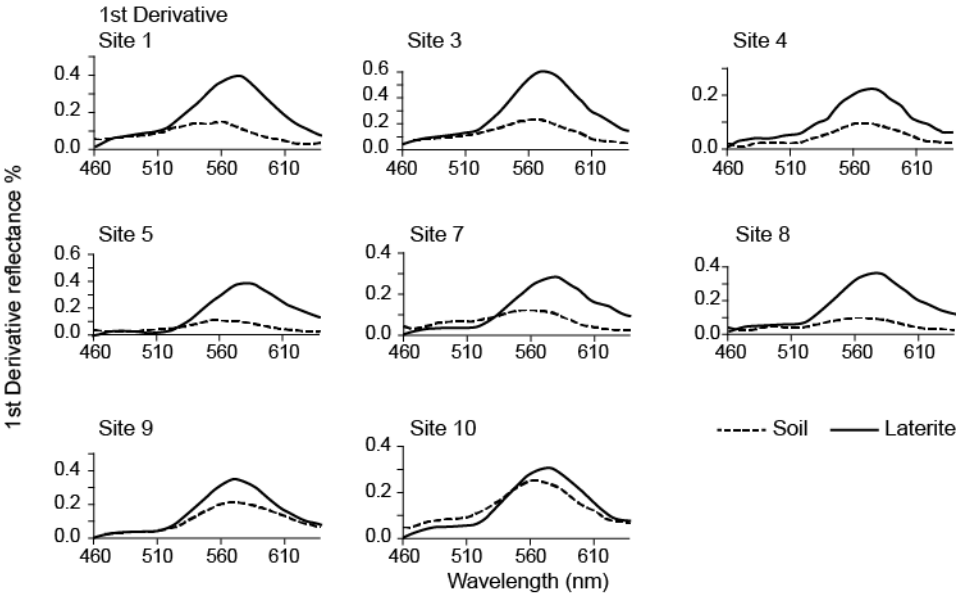

Figure 9. DRS. First Derivative results (D 1), for haematite in paired laterites and soils. Site locations shown on Figure 2.

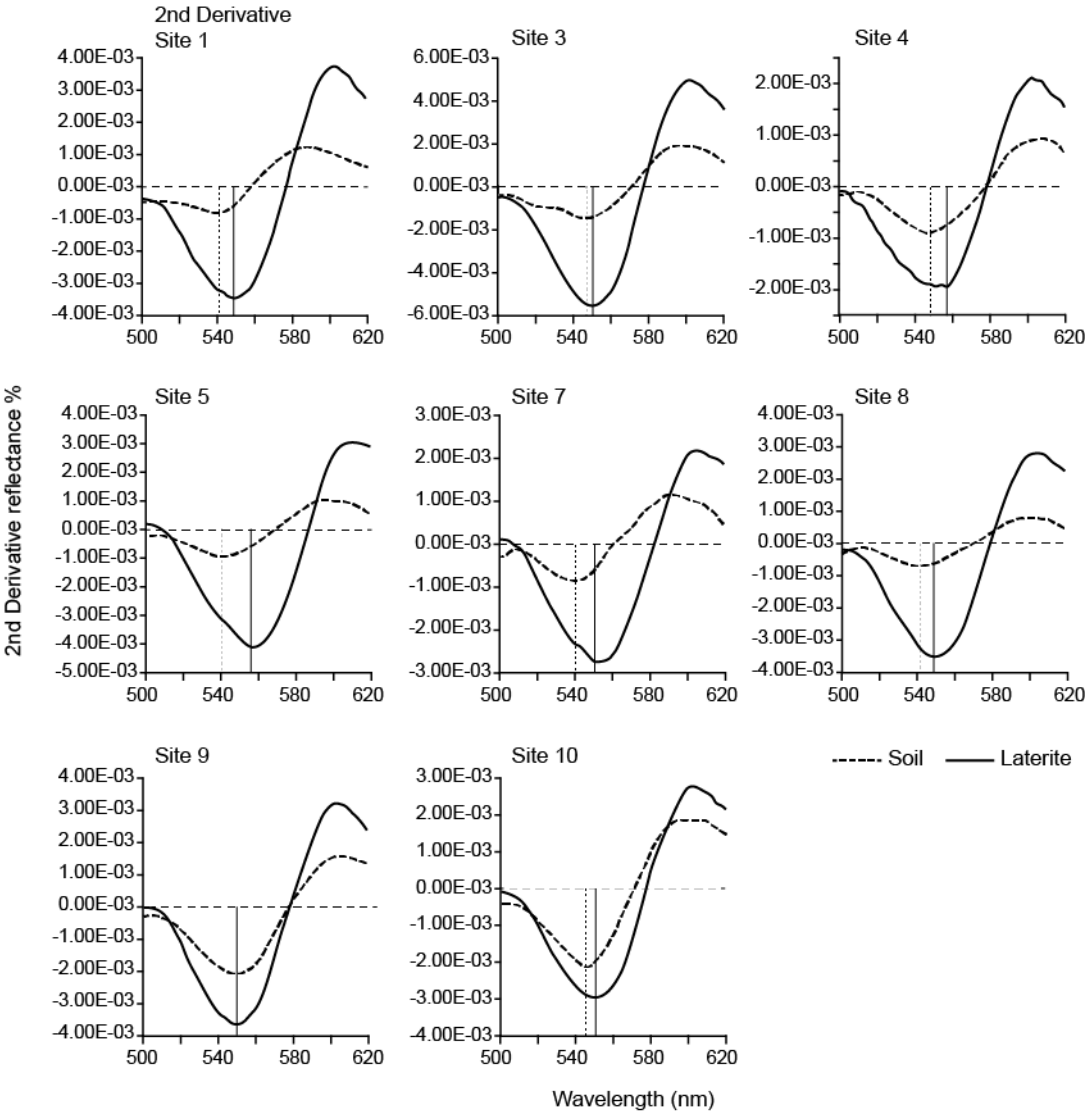

Figure 10. DRS. Secod Derivative (D 2) results for haematite in paired laterites and soils . Vertical lines pass through the minimum wavelength for each sample. Site locations shown on Figure 2.

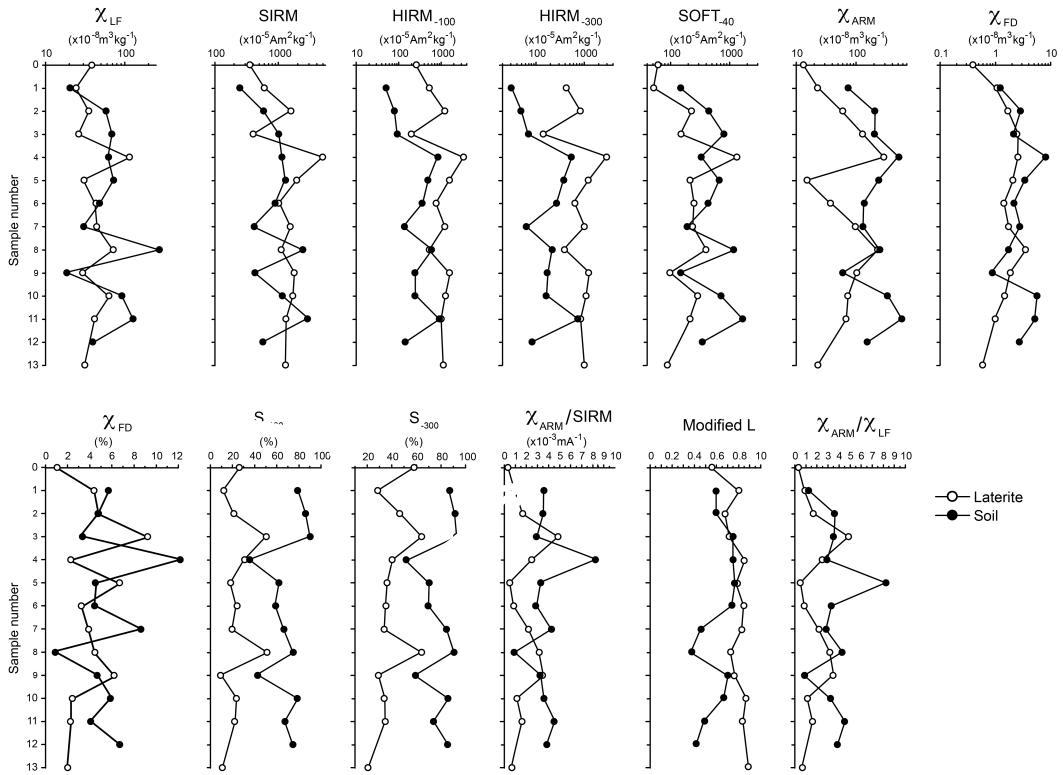

Magnetic properties of laterite and soil samples between Niamey (Niger) and Ouagadougou (Burkina Faso)

Figure 11. Results of magnetic measurements of all of the samples from the transect.

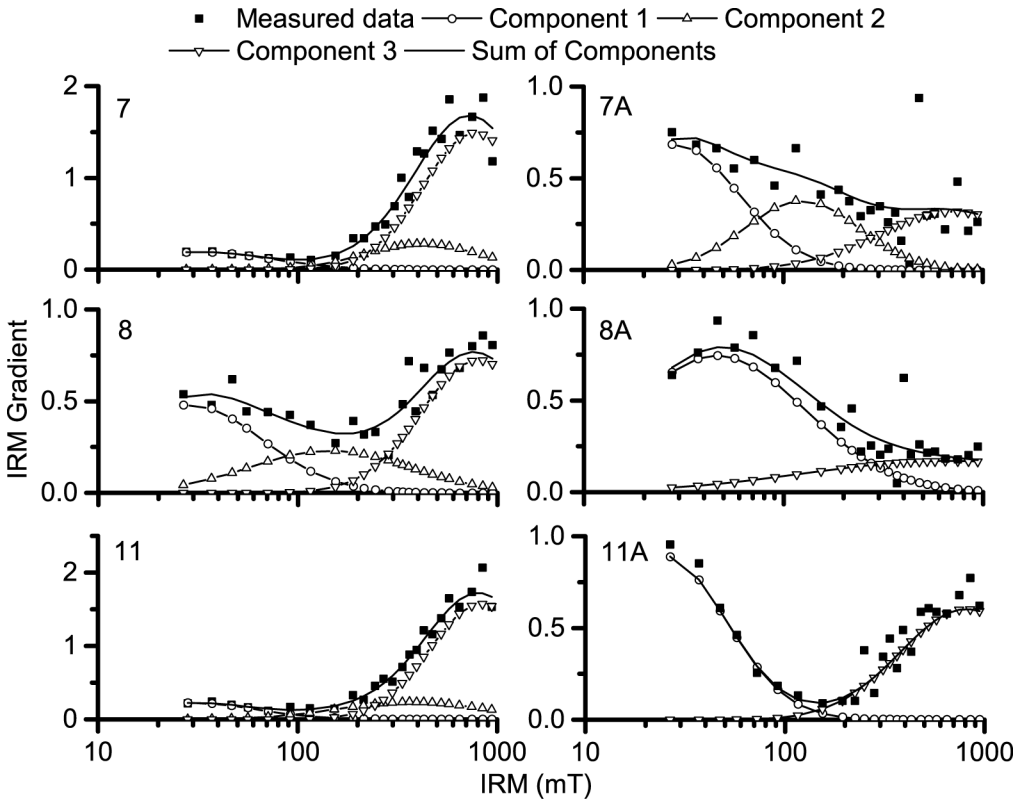

Figure 12. IRM acquisition - deconvolution plots. Site locations shown on Figure 2.